RSC Advances

PAPER

View Article Online
View Journal | View Issue

Cite this: *RSC Adv.*, 2025, **15**, 47913

Dispersive solid phase extraction using SiO_2@ZIF-8@Fe_3O_4 core–shell nanoparticles for extraction of Cd(II), Zn(II), and Cu(II) ions from fruit juice samples

Zohreh Saeedi,[a] Saeed Mohammad Sorouraddin, *[a] Mir Ali Farajzadeh, [ab] Mohammad Reza Afshar Mogaddam [cde] and Atefeh Bakhshi[a]

Monitoring heavy metal contaminations in food and beverage products is essential for ensuring public health. However, most existing extraction techniques suffer from low selectivity, limited sensitivity, and time-consuming sample preparation steps. To overcome these limitations, a dispersive micro solid phase extraction (D-μSPE) method was developed using SiO_2@ZIF-8@Fe_3O_4 core–shell nanoparticles; a composite material that combines high surface area, magnetic separation capability, and chemical stability, and has not been previously applied for this purpose. The synthesized nanocomposite was employed for the adsorption of Cd(II), Cu(II), and Zn(II) ions from fruit juice samples, followed by desorption with diluted nitric acid solution and quantification by flame atomic absorption spectrometry. The main experimental parameters including sorbent amount, extraction and desorption times, solvent type and volume, pH, and salt addition were systematically optimized. Under optimized conditions, the linear ranges of the calibration curves were established in the ranges of 0.5–100, 0.8–80 and 1.2–75 μg L^{-1}, for Zn(II), Cu(II), and Cd(II) ions, respectively. The detection limits were found to be 0.4, 0.3 and 0.2 μg L^{-1} along with the extraction recoveries of 95.2, 96.8, and 98.1% for Cd(II), Cu(II), and Zn(II) ions, respectively. The repeatability of the established method, indicated by relative standard deviation, was less than 5% for intra-day (C = 25 μg L^{-1}, n = 6) and inter-day (C = 25 μg L^{-1}, n = 4) precisions. The developed approach was successfully applied to various commercial fruit juice samples and validated using a certified reference material. This study introduced a rapid, low-cost, and eco-friendly strategy for trace-level monitoring of heavy metals in food matrices, highlighting its strong potential for routine food quality control and public health protection.

Received 10th September 2025
Accepted 25th November 2025

DOI: 10.1039/d5ra06835e

rsc.li/rsc-advances

1. Introduction

Heavy metals have become a significant environmental concern due to their persistent nature and toxic effects on living organisms.[1] These metals are often released into ecosystems through industrial processes, agricultural activities, and waste disposal. They can accumulate in soil, water, and living organisms, leading to severe ecological and health hazards. Copper, cadmium, and zinc are among the most concerning heavy metals.[2] Each of these metals poses unique risks to human health. Copper, is essential in trace amounts for various biological functions, however it can be toxic in higher concentrations, leading to gastrointestinal distress and neurological issues.[3,4] Cadmium is particularly harmful, being linked to kidney damage, bone fragility, and an increased risk of cancer.[5] Zinc, is necessary for immune function and cellular metabolism, but it can also exhibit toxicity at elevated levels, resulting in nausea, vomiting, and impaired immune response.[6]

Given the potential hazards associated with these heavy metals, it is crucial to monitor their concentrations in food and environmental samples. Accurate measurement can be achieved using various analytical instruments such as flame atomic absorption spectroscopy (FAAS),[7–9] inductively coupled plasma (ICP) – optical emission spectroscopy,[10,11] and ICP – mass spectrometry.[12–14] FAAS due to its advantages such as simplicity, cost-effectiveness, and ability to provide rapid results with high sensitivity is more preferable interest.[15,16] However, the complexity of samples and low concentration of analytes often necessitate sample preparation methods to enhance the accuracy, reliability, and sensitivity of analysis.[17,18] For this purpose, various methods can be used such as liquid–liquid

[a]*Department of Analytical Chemistry, Faculty of Chemistry, University of Tabriz, Tabriz, Iran. E-mail: saied_sorour@yahoo.com; ssoroureddin@tabrizu.ac.ir; Fax: +98 41 33334019; Tel: +98 41 33393110*

[b]*Engineering Faculty, Near East University, Mersin 10, 99138 Nicosia, North Cyprus, Turkey*

[c]*Food and Drug Safety Research Center, Pharmaceutical Sciences Institute, Tabriz University of Medical Sciences, Tabriz, Iran*

[d]*New Material and Green Chemistry Research Center, Khazar University, 41 Mehseti Street, Baku AZ1096, Azerbaijan*

[e]*Pharmaceutical Analysis Research Center, Pharmaceutical Sciences Institute, Tabriz University of Medical Sciences, Tabriz, Iran*

extraction,[19,20] liquid phase microextraction methods,[21–23] solid phase extraction (SPE),[24–26] solid phase microextraction,[24] and dispersive SPE (D-μSPE).[27–29] In previous studies, various extraction and preconcentration techniques were explored for the removal and determination of heavy metals in food and environmental matrices. Conventional LLE and SPE methods were widely used owing to their acceptable recoveries; however, they generally require large volumes of toxic solvents, multiple preparation steps, and long extraction time. To overcome these limitations, advanced sorbent materials such as graphene oxide, activated carbon, ion-exchange resins, metal–organic frameworks (MOFs), and magnetic nanocomposites have been developed to improve extraction efficiency, selectivity, and environmental compatibility. Zeolitic imidazolate framework (ZIF-8) has gained attention due to its high porosity, tunable pore size, and strong metal–ligand interactions, which enable effective adsorption of heavy metal ions.[30–32] Nevertheless, pristine ZIF-8 often suffers from limited stability in aqueous media and poor recyclability. The integration of Fe_3O_4 magnetic nanoparticles provides facile magnetic separation, while silica coating (SiO_2) further enhances the structural stability and surface functionality of the composite. The ZIF-8@Fe_3O_4 hybrid structure was successfully used for the removal of Cu^{2+} ions from aqueous systems, demonstrating strong affinity and rapid magnetic separation capability.[33] Similarly, ZIF-8@Fe_3O_4 composite was shown excellent performance in the simultaneous removal of Pb(II) and Cu(II) ions from water, confirming its high adsorption efficiency and reusability.[34] In addition, a SiO_2@ZIF-8@Fe_3O_4 nanocomposite was recently reported for the efficient adsorption of insecticides, highlighting the multifunctional nature and surface versatility of silica-coated magnetic ZIF-8 materials.[35]

Despite the promising potential of such hybrid nanomaterials, few studies have investigated their performance in complex food matrices such as fruit juices, where the presence of organic compounds and natural acids can hinder extraction performance. Therefore, the development of a robust, magnetically separable, and highly selective nanocomposite sorbent is essential for accurate determination of trace metals in real food systems. In recent years, a wide range of nanocomposite sorbents were developed to enhance the efficiency and selectivity of extraction methods for heavy metal ions. Carbon-based materials such as activated carbon, graphene oxide, and biochar have shown strong adsorption capacities due to their large surface areas and functional groups,[36–41] but they often suffer from poor regeneration and weak magnetic responsiveness. MOFs and ZIFs have gained growing attention because of their tunable pore structures, high porosity, and strong affinity toward metal ions. However, pristine MOFs are often unstable in aqueous environments and difficult to separate from solution after extraction. To overcome these drawbacks, hybrid nanocomposites integrating MOFs or ZIFs with magnetic cores (Fe_3O_4) and inorganic supports (*e.g.*, SiO_2, TiO_2 or Al_2O_3) were proposed. These multifunctional materials combine the high surface area of MOFs with the easy magnetic recovery of Fe_3O_4 and the structural robustness of silica, making them ideal for preconcentration of trace metals and organic pollutants in complex matrices. Furthermore, recent studies have highlighted the potential of MOF-based magnetic nanocomposites for the removal of contaminants such as Pb(II), Ni(II), and Cr(VI) ions from aqueous and food samples, showing significant improvements in adsorption capacity and reusability.[42–44] These advancements underline the importance of designing multifunctional hybrid sorbents, such as SiO_2@ZIF-8@Fe_3O_4, for efficient and eco-friendly extraction of toxic metals from food matrices.

In D-μSPE, dispersion of a sorbent into the solution containing analytes increases the potential interactions and contact area between the analytes and sorbent significantly. It results in short extraction time and high extraction efficiency. The structure and type of the desired sorbent are important parameters for successful DSPE. The parameters to consider when choosing a sorbent include: high selectivity, ease of preparation, sorption capacity, and stability. Therefore, different sorbents based on graphene oxide,[45] metal–organic framework,[46] buckytubes,[47] cobalt ferrite nanoparticles,[48] silica gel,[49] porous carbon,[50] and polythiophene[51] were used in the extraction of heavy metal ions. D-μSPE has advantageous due to its efficiency in isolating target analytes from complex matrices while minimizing solvent usage and time.[52–54]

In this study, a developed D-μSPE method using SiO_2@ZIF-8@Fe_3O_4 sorbent was used to extract heavy metal ions from fruit juice samples. This composite combined magnetic iron oxide (Fe_3O_4) with zeolitic imidazolate frameworks[55] and silica to provide a unique structure with enhanced adsorption capability while facilitating easy separation from the sample matrix. Also, the magnetic properties of Fe_3O_4 allowed for rapid recovery of the adsorbent after extraction, while ZIF-8 contributed to high surface area. The silica component further stabilizes the structure and enhances its compatibility with various solvents. According to our knowledge, the ability of this sorbent was not studied in the extraction of heavy metal ions till now. Through this approach, we aim to significantly advance the methods used for detecting heavy metals in environmental samples. By integrating FAAS with the D-μSPE process based on SiO_2@ZIF-8@Fe_3O_4 sorbent low detection limits and enhanced selectivity for the targeted analytes were achieved. This research not only addressed the pressing need for effective monitoring of heavy metals but also demonstrated the potential of advanced materials in enhancing analytical techniques for food safety and public health protection.

2. Experimental

2.1. Chemicals and reagents

A standard solution containing 100 mg L^{-1} of each Cd(II), Cu(II), and Zn(II) ion was prepared in deionized water using $Cd(NO_3)_2 \cdot 4H_2O$, $Cu(NO_3)_2 \cdot 3H_2O$, and $Zn(NO_3)_2 \cdot 6H_2O$ (Merck, Darmstadt, Germany). It was diluted with deionized water to the concentration of 50 μg L^{-1} of each ion and used as a working solution during optimization steps. Iron(III) chloride hexahydrate ($FeCl_3 \cdot 6H_2O$), sodium diethyldithiocarbamate (SDDTC) (as a complexing agent), sodium acetate hexahydrate, HCl solution (37%, w/w), HNO_3 solution (65%, w/w), ethylene glycol,

triethylamine, methanol, cetyltrimethylammonium bromide, tetraethoxysilane, concentrated ammonia solution (25%, w/w), 2-methylimidazole, disodium hydrogen phosphate, phosphoric acid, and acetonitrile were purchased from Merck. All of the chemicals were the highest purity grade available commercially.

2.2. Real samples

Seven fruit juice samples (cherry, mango, pineapple, grapefruit, pomegranate, kiwi, and apple) produced by various domestic producers were bought from local supermarkets (Tabriz, East Azerbaijan, Iran). The juices were thoroughly homogenized before subsampling and stored at 4 °C until analysis.

2.3. Instrumentation

The analytes were determined using a Shimadzu-6300 Flame Atomic Absorption Spectrometer (Kyoto, Japan) equipped with a deuterium lamp for background correction. The radiation sources included hollow-cathode lamps of zinc, cadmium, and copper (Hamamatsu Photonics, Japan), operating at 15, 10, and 15 mA at the wavelengths of 228.8, 324.8, and 307.6 nm, and the spectral resolutions of 0.5, 0.5, and 0.7 nm, respectively. The analytical signal for quantification was based on peak height. Acetylene and air flow rates set at 2.3 and 15.0 L min^{-1}, respectively were used as fuel and oxidant for flame. A Fourier Transform Infrared Spectrometer (FTIR, Bruker, USA) was used to obtain the FTIR spectrum. The surface morphology of the sorbent was analyzed using a scanning electron microscope (SEM). An X-ray diffractometer (D500) recorded the X-ray diffraction (XRD) pattern. Moreover, energy-dispersive X-ray (EDX) analysis (MIRA3 FESEM, TESCAN, Czech) was applied for studying the elemental composition. The ultrasonic bath device made in Germany (60H Elmasonics) and Labinco L46 vortex mixer (Netherlands) were used. pH measurements were conducted using a Metrohm pH metre model 654, manufactured in Herisau, Switzerland.

2.4. Synthesis of sorbent

2.4.1. Preparation of Fe_3O_4 nanoparticles. Fe_3O_4 nanoparticles were prepared using a solvothermal technique previously described in literature with slight modifications.[56] 0.95 g of $FeCl_3 \cdot 6H_2O$ and 4.2 g of $CH_3COONa \cdot 6H_2O$ were dissolved in 50 mL of ethylene glycol, stirred for 20 min, and then subjected to sonication for 30 min. It was transferred into a stainless-steel autoclave and heated at 250 °C for 6 h. After cooling, the resulting black magnetic solid was separated using an external magnet. Finally, the obtained black solid was washed with deionized water and ethanol at least three times and thoroughly dried in an oven.

2.4.2. Synthesis of ZIF-8@Fe_3O_4. 0.2 g of Fe_3O_4 and 2 g of $Zn(NO_3)_2 \cdot 6H_2O$ were added into 12 mL of deionized water and stirred until the salt is completely dissolved (solution A). Next, solution B was prepared by dissolving 2.2 g of 2-methylimidazole and 1 mL of triethylamine in 48.5 mL of deionized water and stirred until they are fully dissolved. Then, quickly solutions A and B were mixed together and stirred vigorously for 1 h. Finally, a gray solid was formed, which separated using an external magnet, washed with deionized water at least three times, and dried in an oven overnight.

2.4.3. Synthesis of SiO_2@ZIF-8@Fe_3O_4. Initially, 0.3 g of cetyltrimethylammonium bromide was dissolved in a mixture of 80 mL deionized water, 60 mL ethanol, and 1.1 mL concentrated ammonia solution. Subsequently, 0.1 g of ZIF-8@Fe_3O_4 was introduced into the solution and subjected to sonication for 15 min. Then, 0.5 mL of tetraethoxysilane was added drop wisely under continuous stirring, and the solution was maintained for 16 h. The obtained gray solid was collected using a magnet, washed with an ethanol/HCl (37%, w/w) (95/5, v/v) mixture to completely remove the surfactant, followed by several washing with ethanol and deionized water. After drying, the final product was obtained and denoted as SiO_2@ZIF-8@Fe_3O_4.

2.5. Extraction procedure

A 7 mL working solution/real sample with a pH of 6 was placed into a 10-mL glass test tube. Then, 12 mg of the synthesized sorbent (SiO_2@ZIF-8@Fe_3O_4) was added and vortexed for 6 min. After removing the sorbent using a magnet, 350 μL of diluted nitric acid solution (5%, v/v) as a desorption solvent was added onto the collected sorbent and vortexed for 3 min. The sorbent was removed in the presence of external magnetic field, and 100 μL of the eluent (for each ion) was taken and injected into FAAS system using a home-made injection system.

3. Results and discussion

3.1. Characterization of sorbent

To confirm the successful synthesis, a series of characterization techniques, including XRD, SEM, EDX, and FTIR were performed. The XRD pattern (Fig. 1A) of ZIF-8 displays sharp and well-defined diffraction peaks at the 2θ range of 10–30°, confirming its high crystallinity and the integrity of its framework structure. For ZIF-8@Fe_3O_4, the characteristic reflections of ZIF-8 are preserved, although with slightly reduced intensity, and weak peaks corresponding to Fe_3O_4 appear in the 30–40° region, indicating the successful encapsulation of Fe_3O_4 within the ZIF-8 matrix. After silica coating, the SiO_2@ZIF-8@Fe_3O_4 composite exhibits a marked decrease in the intensity of crystalline peaks, accompanied by a broad diffuse band around 20–25°, which is characteristic of amorphous SiO_2, confirming the formation of a silica layer over the composite surface.

The SEM image of ZIF-8@Fe_3O_4 (Fig. 1B) shows well-defined, submicron polyhedral particles with relatively uniform morphology and clear faceted surfaces, consistent with ZIF-8 growth on magnetic cores. The particles appear to form aggregates while maintaining distinct faceted outlines, indicating that the ZIF-8 shell is crystalline and sufficiently thick to define the particle shape. The surface texture and particle packing suggest successful deposition of ZIF-8 around the magnetic cores without significant collapse or sintering. The SEM image of SiO_2@ZIF-8@Fe_3O_4 (Fig. 1C) reveals that the original faceted morphology is preserved but the particle surfaces are noticeably

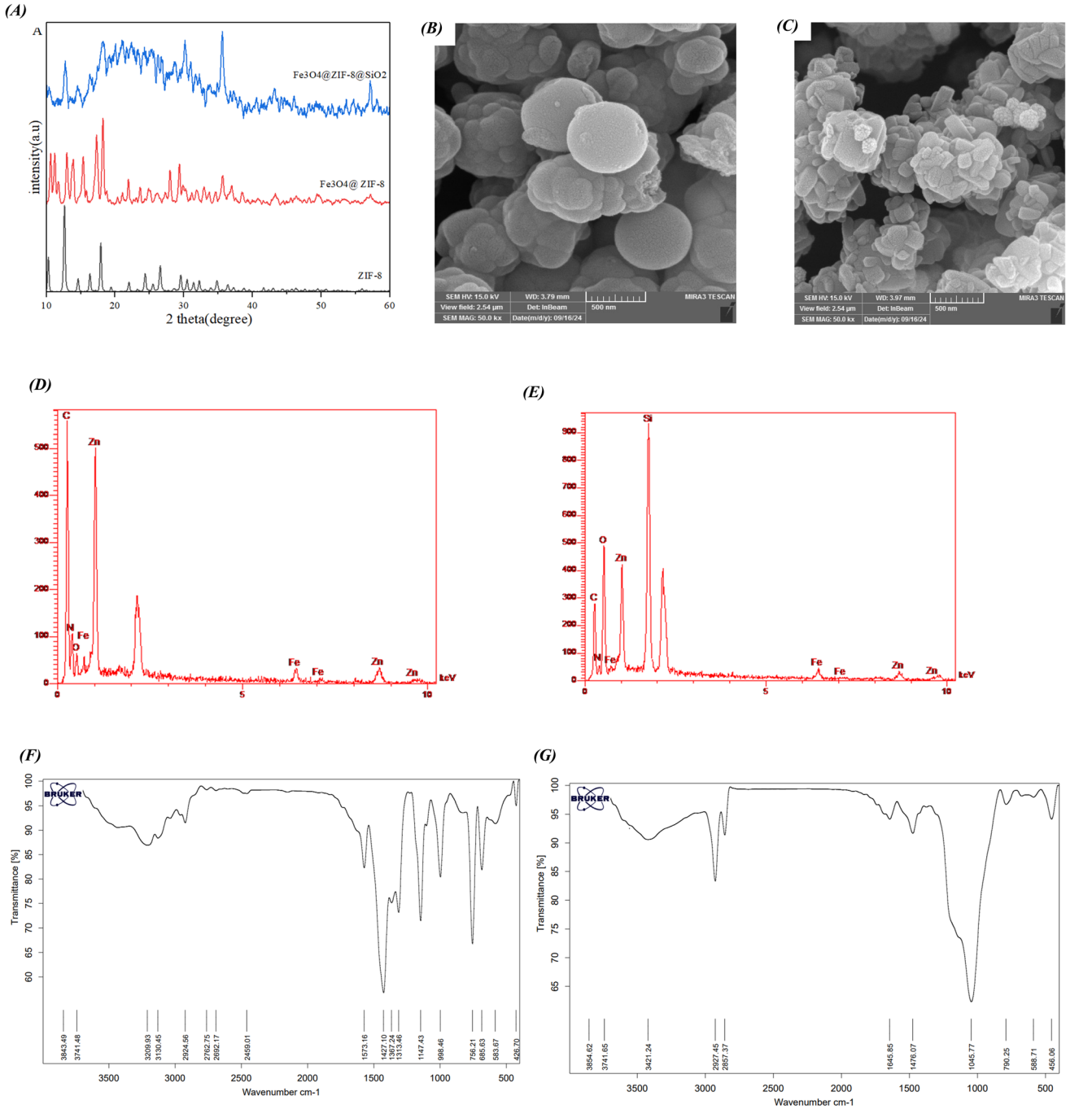

Fig. 1 (A) XRD patterns of ZIF-8, ZIF-8@Fe_3O_4, and SiO_2@ZIF-8@Fe_3O_4, (B) SEM image of ZIF-8@Fe_3O_4, (C) SEM image of SiO_2@ZIF-8@Fe_3O_4, (D) EDX spectrum of ZIF-8@Fe_3O_4 (E) EDX spectrum of SiO_2@ZIF-8@Fe_3O_4, (F) FTIR spectrum of ZIF-8@Fe_3O_4, and (G) FTIR spectrum of SiO_2@ZIF-8@Fe_3O_4.

smoother and slightly more rounded, consistent with the formation of an amorphous silica overlayer. The silica coating reduces the visibility of ZIF-8 facets and increases particle cohesion, yielding more compact aggregates. No obvious fragmentation or destruction of the underlying core–shell structure is observed, indicating that the silica deposition proceeded conformally and gently.

EDX was employed to investigate the elemental composition of the synthesized adsorbent in stages 3 and 4 of the preparation processes (Sections 2.4.2 and 2.4.3). In the case of Fe_3O_4@ZIF-8, the EDX spectrum (Fig. 1D) shows the presence of C, N, and O, originating from the ligand of 2-methylimidazole in the ZIF-8 framework, along with distinct Zn peaks confirming the successful incorporation of zinc into the metal–organic framework. Fe peaks are also detected, corresponding to the Fe_3O_4 core, and the relatively higher intensity of Zn and C peaks compared to Fe peak indicates effective coating of the Fe_3O_4 nanoparticles with the ZIF-8 shell. In the case of SiO_2@ZIF-

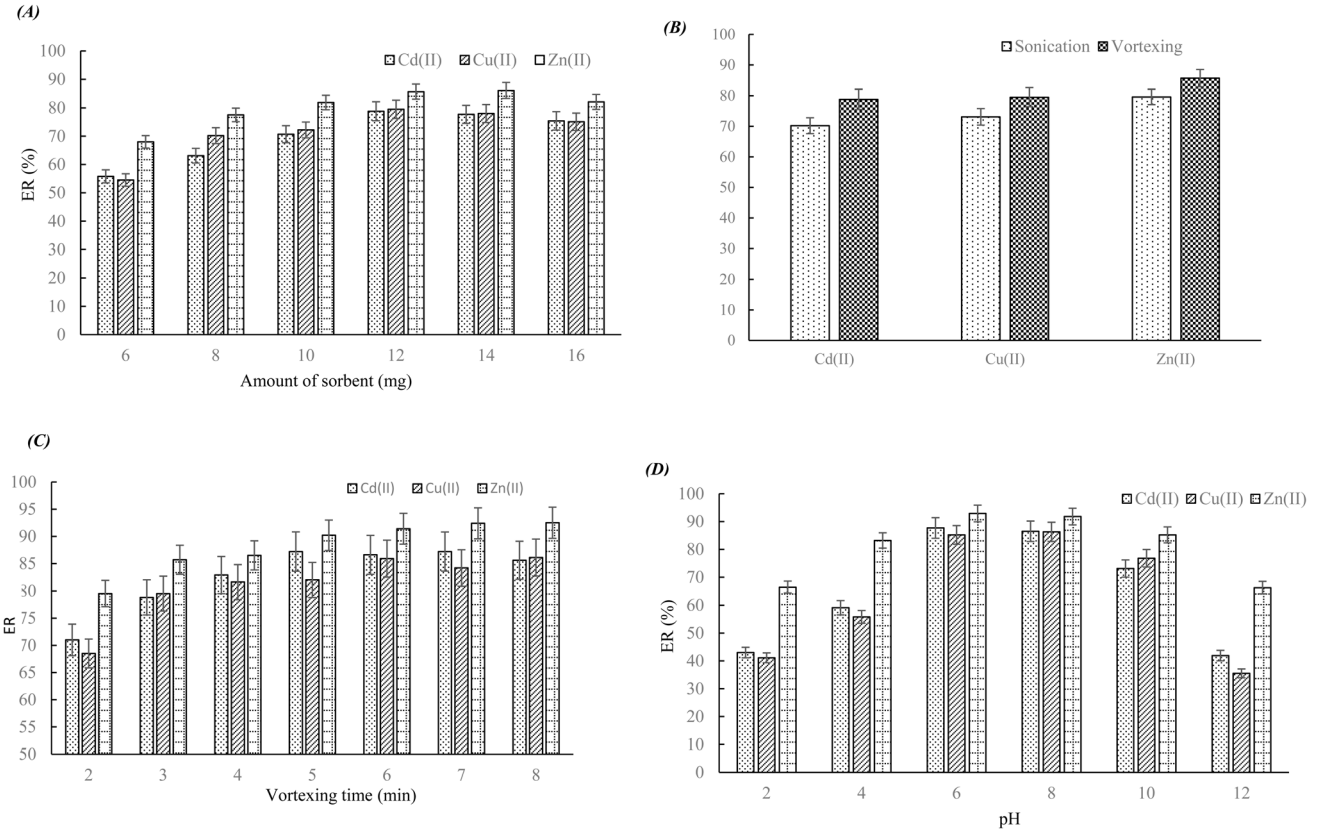

Fig. 2 (A) Optimization of sorbent amount. Extraction conditions: sample; 7 mL of deionized water containing 50 μg L^{-1} of each Cd(II), Cu(II), and Zn(II) ion; extraction time, 3 min; and desorption solvent (volume), HNO_3 5% v/v (300 μL). (B) Study of agitation type in adsorption step. Extraction conditions: sorbent amount 12 mg was selected; the other circumstances were mentioned in (A). (C) Optimization of time of vortexing during adsorption step. Extraction conditions were the same as those used in (B), except vortexing was used for the agitation. (D) Optimizing of pH. Extraction conditions: extraction time was selected 6 min, and the other conditions were as the same those utilized in (B).

8@Fe_3O_4, the EDX spectrum (Fig. 1E) reveals, in addition to C, N, O, Zn, and Fe peaks, a prominent Si peak at approximately 1.7 keV, confirming the successful deposition of the SiO_2 layer. The marked increase in oxygen content compared to Fig. 1D is attributed to the presence of Si–O bonds in the silica shell, while the reduced relative intensity of Fe peak suggests complete encapsulation of the Fe_3O_4 core and ZIF-8 shell by the silica coating. These findings confirm the successful fabrication of the SiO_2@ZIF-8@Fe_3O_4 composite with a magnetic core, metal–organic framework shell, and protective silica layer.

FTIR analysis was performed to confirm the functional groups and structural changes in the synthesized materials during Sections 2.4.2 and 2.4.3 of the fabrication process. In the case of ZIF-8@Fe_3O_4 (Fig. 1F), the characteristic absorption bands of ZIF-8 are observed, including peaks at 1573 and 1427 cm^{-1} corresponding to C=N stretching and C–N stretching vibrations of the imidazole ring, respectively. The band near 1147 cm^{-1} is attributed to in-plane bending of the imidazole, while peaks at 998 and 756 cm^{-1} are associated with out-of-plane bending of the imidazole ring. The absorption band at ~426 cm^{-1} corresponds to the Fe–O vibration, confirming the presence of the Fe_3O_4 core within the composite. The peak observed around 1147 cm^{-1} corresponds to in-plane bending of the imidazole ring, while those near 998 and 756 cm^{-1} are due to out-of-plane and ring deformation vibrations, confirming the presence of the ZIF-8 framework. The weak band at approximately 2900 cm^{-1} is assigned to C–H stretching vibrations from the imidazole ligand and residual organic moieties. After silica coating, the relative intensity of the imidazole-related peaks (756–1147 cm^{-1}) decreases slightly, whereas a new broad and strong band appears near 1045 cm^{-1}, corresponding to Si–O–Si asymmetric stretching, and a small band near 790 cm^{-1} due to Si–O–Si symmetric stretching. These spectral changes indicate successful formation of the SiO_2 shell and partial masking the ZIF-8 surface functional groups by the silica network, confirming the transformation from ZIF-8@Fe_3O_4 to SiO_2@ZIF-8@Fe_3O_4 composite. In the case of SiO_2@ZIF-8@Fe_3O_4 (Fig. 1G), the FTIR spectrum exhibits all the characteristic bands of ZIF-8, along with a new strong and broad absorption band centered around 1045 cm^{-1}, which is assigned to the Si–O–Si asymmetric stretching vibration, indicating successful coating with silica. The small band near 790 cm^{-1} is attributed to symmetric stretching of Si–O–Si bonds, further confirming the silica shell formation. The Fe–O vibration at 588 cm^{-1} is still present but with reduced relative intensity due to the silica encapsulation. These spectral changes clearly demonstrate the

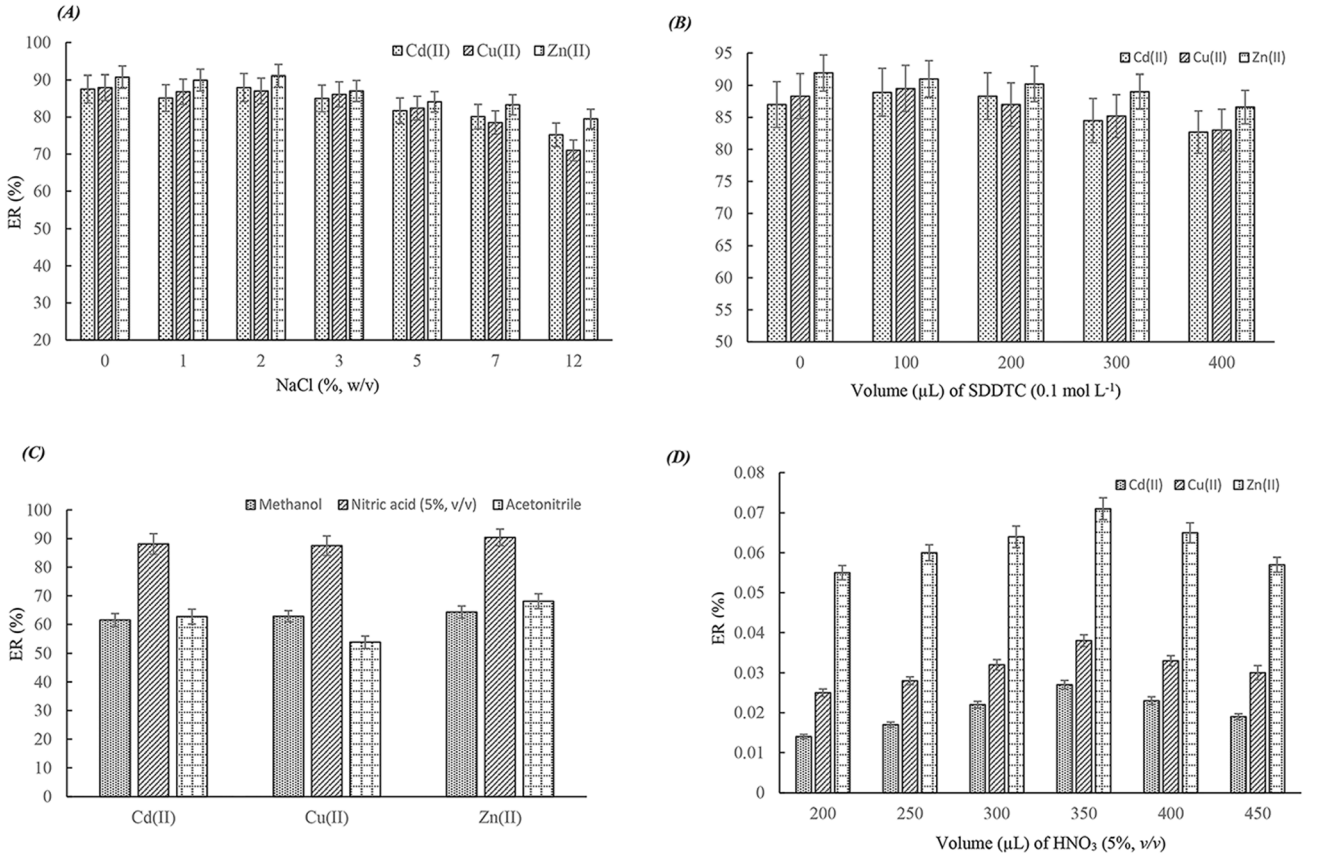

Fig. 3 (A) Study of the effect of salt addition. Extraction conditions were as the same of those used in Fig. 2D, except no pH adjustment was done, (B) study the effect of complexing agent volume. Extraction conditions are the same as those utilized in (A), except no salt was added. (C) Examining desorption solvent type. Extraction conditions were the same as those used in (B), except no complexing agent was used (D) optimizing of volume of HNO_3 (5%, v/v). Extraction circumstances are the same as those used in (C), except nitric acid 5% (v/v) was used as the elution solvent.

stepwise assembly of the SiO_2@ZIF-8@Fe_3O_4 composite with a silica-protected outer surface.

3.2. Formation mechanism of SiO_2@ZIF-8@Fe_3O_4

The synthesis of the composite follows a stepwise core–shell self-assembly mechanism. Initially, Fe_3O_4 nanoparticles act as magnetic cores bearing abundant surface –OH groups, which facilitate hydrogen bonding and electrostatic interactions with the silica precursor (TEOS) during hydrolysis–condensation, leading to the formation of a thin and uniform SiO_2 layer around Fe_3O_4. This silica coating not only enhances the dispersion stability of Fe_3O_4 but also introduces surface silanol (Si–OH) groups that serve as nucleation sites for subsequent ZIF-8 growth. Upon the addition of 2-methylimidazole and Zn^{2+} ions, coordination occurs between Zn^{2+} and the nitrogen atoms of 2-methylimidazole ligands at the SiO_2 surface, initiating heterogeneous nucleation and growth of the ZIF-8 shell. The interfacial bonding between Si–OH groups and Zn–N coordination frameworks stabilizes the attachment of the MOF layer. The resulting hierarchical core–shell architecture comprises a magnetic Fe_3O_4 core for facile magnetic separation, an intermediate ZIF-8 layer for its high surface area, and an outer SiO_2 shell that provides active sites for metal-ions adsorption.

This composite is thus formed through a combination of electrostatic attraction, coordination bonding, and controlled crystallization, yielding SiO_2@ZIF-8@Fe_3O_4 nanostructures with excellent structural integrity and functional performance.

Table 1 Tolerance limits of interferent/analyte ratios of the studied coexisting ions in determination of Cd(II), Cu(II), and Zn(II) ions by using the proposed method

	Tolerance limit of interferent : analyte ratio		
Species	Cd(II)	Cu(II)	Zn(II)
Pb^{2+}	500	500	750
Al^{3+}	1250	1500	1500
Fe^{3+}	1000	1000	1500
Pd^{2+}	1500	1500	1000
Co^{2+}	400	300	500
Ni^{2+}	500	400	800
Mn^{2+}	400	400	500
Na^{+}	2000	2000	1500
K^{+}	2000	2000	2000
Ca^{2+}	1250	1500	1250
Mg^{2+}	1500	2000	2000
Hg^{2+}	200	200	200
Ag^{+}	1750	1750	2000
SO_4^{2-}	2000	2000	2000
NO_3^{-}	3000	2750	3500

Table 2 Quantitative characteristics of the proposed method for the analysis of Cd(II), Cd(II), and Zn(II) ions

Analyte	LR[a] (μg L^{-1})	r^{2b}	LOD[c] (μg L^{-1})	LOQ[d] (μg L^{-1})	[e]RSD%		ER ± SD[f]
					Intra-day ($n = 6$)	Inter-day ($n = 4$)	
Cd(II)	1.2–75	0.994	0.4	1.2	4.0	4.9	95.2 ± 3.8
Cu(II)	0.8–80	0.992	0.3	0.8	3.8	4.8	96.8 ± 3.7
Zn(II)	0.5–100	0.997	0.2	0.5	3.1	3.7	98.1 ± 3.0

[a] Linear range. [b] Coefficient of determination. [c] Limit of detection. [d] Limit of quantification. [e] Relative standard deviation ($C = 25$ μg L^{-1} of each cation). [f] Extraction recovery ± standard deviation ($n = 3$).

Table 3 Analysis of SPS-WW2 Batch 108 (CRM) for the determination of Cd(II), Cu(II), and Zn(II) ions with the developed method

Cation	Certified concentration (μg L^{-1}) ± S.D.[a] ($n = 3$)	Found concentration (μg L^{-1}) ± S.D. ($n = 3$)	t-Test[b]
Cd(II)	100 ± 0.5	94.4 ± 4.3	2.25
Cu(II)	2000 ± 10	2147.8 ± 94.4	2.71
Zn(II)	3000 ± 15	3108.7 ± 102.6	1.83

[a] Standard deviation. [b] $t_{0.05,2} = 4.30$.

The gradual diffusion of Zn^{2+} and 2-methylimidazole toward the SiO_2 surface promotes controlled nucleation rather than bulk precipitation, ensuring a uniform and compact layer.

3.3. Optimization of extraction procedure

3.3.1. Optimization of SiO_2@ZIF-8@Fe_3O_4 amount. A crucial factor to optimize is the amount of sorbent, since the number of adsorption sites has a direct impact on the extraction efficiency. This section investigated how varying the amount of sorbent from 6 to 16 mg affects analytes adsorption. As illustrated in Fig. 2A, increasing the sorbent quantity up to 12 mg leads to enhanced extraction recoveries (ERs) for all analytes attributed to an increase in available adsorption sites. However, when the sorbent amount surpasses 12 mg, ERs approximately constant and thereafter decline, likely due to the aggregation of the sorbent particles. Therefore, 12 mg was identified as the optimal sorbent quantity.

3.3.2. Type and time of stirring during adsorption step. In this section, two stirring techniques; vortexing and sonication (at the same time, 3 min) were utilized to disperse the sorbent particles into the solution, aiming to maximize the interactions between the analytes and sorbent. The findings (Fig. 2B) show that vortexing resultes in higher ERs of the analytes compared to sonication. It appears that vortexing enhances dispersion of the sorbent into the solution. Based on these results, vortexing was chosen for the stirring process during the adsorption step. The next factor was the duration of vortexing, which influences the extraction (adsorption) time. A time range of 2 to 8 min was investigated to optimize this duration. As indicated in Fig. 2C, ERs increase from 2 to 6 min of adsorption time and then remain constant. Since 6 min provides sufficient opportunity for interactions between the analytes and sorbent, extending the time do not further improve ERs. Thus, the optimal extraction time was determined to be 6 min.

3.3.3. Study of pH. The next significant factor affecting efficiency of the extraction of the analytes in this study can be pH of solution, as it directly influences the forms of the analytes and stability of the sorbent. To achieve effective extraction, the impact of pH was assessed by adding 0.1 mol L^{-1} solution of sodium hydroxide or hydrochloric acid into the solution. The pH range studied was from 2 to 12. According to the results (Fig. 2D), the highest ERs are observed at pHs 6 and 8. As pH increases more than 8, a decrease in ERs is observed owing to the formation of hydroxide complexes or precipitates of the studied cations. The pH of the samples used was in this range, therefore, the original aqueous samples were used without any pH adjustment.

3.3.4. Study of salt addition. The addition of a salt can influence extraction efficiency in two ways. Firstly, increasing the ionic strength of aqueous solution decreases solubility of the analytes, which can improve extraction efficiency. Secondly, adding salt increases viscosity of the aqueous solution, which reduces both diffusion coefficients and ERs of the analytes. To evaluate the impact of salt addition on ERs of the analytes, different concentrations of NaCl (0, 1, 2, 3, 5, 7, and 12%, w/v) were added to the working solution. The findings (Fig. 3A) reveal that NaCl do not have a positive effect on the ERs, thus, salt addition was excluded from the further tests.

3.3.5. Effect of complexing agent concentration. The extraction efficiency of the method can be improved when the selected ions are complexed with a suitable chelating agent, because the formed complexes may be adsorbed onto the surface of adsorbent more than the heavy metal ions. To investigate this issue, SDDTC was selected to induce complexation of the selected ions. Therefore, the effect of SDDTC concentration on the ERs of Cd(II), Cu(II), and Zn(II) ions was investigated by changing the volume of SDDTC solution (0.1 mol L^{-1}) from 0 to 400 μL. The results in Fig. 3B show that

Table 4 Results of assays in determination of concentrations of Cd(II), Cu(II), and Zn(II) ions in the selected fruit juice samples and checking sample matrices effect

Analyte	Spiked concentration (μg kg^{-1})	Cherry juice: Found concentration (μg kg^{-1}) ± S.D. ($n = 3$)	Cherry juice: RR[a] ± S.D.[b] ($n = 3$)	Mango juice: Found concentration (μg kg^{-1}) ± S.D. ($n = 3$)	Mango juice: RR ± S.D. ($n = 3$)	Pineapple juice: Found concentration (μg kg^{-1}) ± S.D. ($n = 3$)	Pineapple juice: RR ± S.D. ($n = 3$)	Grapefruit juice: Found concentration (μg kg^{-1}) ± S.D. ($n = 3$)	Grapefruit juice: RR ± S.D. ($n = 3$)	Pomegranate juice: Found concentration (μg kg^{-1}) ± S.D. ($n = 3$)	Pomegranate juice: RR ± S.D. ($n = 3$)	Kiwi juice: Found concentration (μg kg^{-1}) ± S.D. ($n = 3$)	Kiwi juice: RR ± S.D. ($n = 3$)	Apple juice: Found concentration (μg kg^{-1}) ± S.D. ($n = 3$)	Apple juice: RR ± S.D. ($n = 3$)
Cd(II)	0	ND[c]	—	6.2 ± 0.4	—	6.5 ± 0.4	—	9.2 ± 0.5	—	ND	—	4.2 ± 0.2	—	ND	—
	10	9.7 ± 0.4	96.7 ± 4.0	15.7 ± 0.7	95.0 ± 4.2	15.9 ± 0.7	94.0 ± 4.0	18.5 ± 0.8	93.0 ± 4.0	9.4 ± 0.4	93.8 ± 4.1	13.6 ± 0.6	94.5 ± 4.1	9.5 ± 0.4	95.4 ± 4.0
	50	48.2 ± 2.0	96.5 ± 3.9	54.5 ± 2.4	96.6 ± 4.2	54.0 ± 2.2	95.0 ± 3.9	56.5 ± 2.5	94.6 ± 4.0	47.6 ± 2.1	95.2 ± 4.1	52.1 ± 2.2	95.8 ± 4.0	47.5 ± 2.0	95.1 ± 4.0
Cu(II)	0	5.5 ± 0.2	—	ND	—	ND	—	28.1 ± 1.1	—	12.8 ± 0.5	—	ND	—	34.8 ± 1.5	—
	10	15.1 ± 0.6	96.2 ± 3.8	9.4 ± 0.4	94.2 ± 4.0	9.6 ± 0.4	96.2 ± 3.9	37.6 ± 1.5	95.4 ± 3.8	22.4 ± 0.9	96.3 ± 4.0	9.6 ± 0.4	96.5 ± 3.8	44.3 ± 1.9	95.0 ± 4.0
	50	54.0 ± 2.1	97.0 ± 3.8	47.3 ± 1.9	94.6 ± 3.7	48.0 ± 1.9	96.0 ± 3.7	76.7 ± 3.1	97.2 ± 3.9	61.8 ± 2.5	98.1 ± 4.0	48.5 ± 2.0	97.1 ± 4.0	82.8 ± 3.3	96.1 ± 3.8
Zn(II)	0	34.2 ± 1.1	—	29.5 ± 1.0	—	21.0 ± 0.7	—	36.2 ± 1.2	—	38.5 ± 1.3	—	31.5 ± 1.0	—	37.1 ± 1.3	—
	10	43.8 ± 1.4	96.5 ± 3.1	39.0 ± 1.3	95.1 ± 3.2	30.7 ± 1.0	96.6 ± 3.1	45.9 ± 1.6	96.8 ± 3.4	48.1 ± 1.6	96.1 ± 3.2	41.1 ± 1.4	96.2 ± 3.2	46.8 ± 1.6	97.1 ± 3.2
	50	82.8 ± 2.6	97.2 ± 3.1	77.4 ± 2.6	95.8 ± 3.2	69.1 ± 2.2	96.2 ± 3.1	84.7 ± 2.8	97.0 ± 3.2	87.1 ± 2.8	97.3 ± 3.1	80.2 ± 2.5	97.5 ± 3.1	85.8 ± 2.8	97.5 ± 3.2

[a] Relative recovery. [b] Standard deviation. [c] Not determined.

adding SDDTC does not have a significant effect on the ERs, and the next experiments were performed without adding any complexing agent.

3.3.6. Optimization of the type and volume of desorption solvent. The extraction efficiency of various potential desorption solvents, including methanol, diluted nitric acid (5%, v/v), and acetonitrile was evaluated to achieve optimal extraction performance. The results (Fig. 3C) indicate that using nitric acid solution (5%, v/v) as the desorption solvent yields the highest extraction efficiency. In this study, the volume of desorption solvent impacts both the extraction efficiency and the analytical sensitivity. Therefore, the role of the nitric acid solution volume in the present study is multifaceted. Firstly, it directly influences the desorption amount of the analytes from the sorbent surface. A larger volume can be result in high desorption. Secondly, the solvent volume affects the analytes concentration in the eluent, which in turn dictates the intensity of the analytical signals in the FAAS system. To elucidate the optimal desorption solvent volume, a series of experiments was performed by varying the volume of nitric acid solution from 200 to 450 μL. The results, presented in Fig. 3D, show that as the solvent volume increases till 350 μL, a concomitant rise in the analytical signals across all target metal ions is observed. Further increases in the volume of the solvent do not augment analytes signal, likely larger volumes began to dilute the analytes. This study show that the higher signals are obtained by 350 μL, and it was selected as the best volume of elution solvent for the next experiments.

3.3.7. Optimizing vortexing time in desorption stage. In this study, the effectiveness of vortexing time during the desorption step was evaluated for maximum possible removal of the analytes from the sorbent surface. A desorption time range of 2–5 min was examined. Increasing the desorption time from 2 to 3 min enhanced extraction efficiency, but extending the time from 3 to 5 min did not result in a significant change in desorption performance. Therefore, 3 min was selected as the optimal desorption time.

3.4. Reusability of sorbent

The capability of the synthesized SiO_2@ZIF-8@Fe_3O_4 sorbent for extracting Cd(II), Zn(II), and Cu(II) ions from working solution was investigated through repeated experiments, where adsorption and desorption steps were performed sequentially according to the "extraction procedure". The data confirmed that the extraction efficiency of the synthesized sorbent remained approximately consistent, with the relative standard deviations (RSDs) between 4.2 and 4.8%, even after using the same sorbent for 5 cycles.

3.5. Effect of coexisting ions

The influence of potential coexisting ions on the ERs of Cd(II), Cu(II), and Zn(II) ions was examined. To do this, 7 mL of working solution containing 50 μg L^{-1} of each Cd(II), Cu(II), and Zn(II) ion was combined with various concentrations of coexisting ions and then the extraction was processed according to the optimized extraction procedure. A studied ion was deemed to

Table 5 Comparison of the proposed method with the other methods used in the extraction, preconcentration, and determination of Cd(II), Cu(II), and Zn(II) ions

Analyte	Method	Sample	LR[a] (μg L^{-1})	LOD[b] (μg L^{-1})	LOQ[c] (μg L^{-1})	RSD[d] (%)	Ref.
Cd(II)	SPE/FAAS[e]	Food samples	5.1–1800	1.5	5.1	<5	57
Zn(II)			4.1–1500	1.2	4.1		
Cd(II)	DSPME[f]/AAS	Water	1–10 mg L^{-1}	0.20	0.68	1.5	58
Zn(II)			1–10 mg L^{-1}	0.26	0.85	1.5	
Cu(II)	DμSPE/EDXRF[g]	Water	1–200	0.06	—	<4.3	59
Zn(II)			1–140	0.07			
Cd(II)	Tetrabutylammonium	Water samples	0.5–160	0.12	—	0.7	60
Cu(II)	bromide aqueous		1–160	0.17		1.3	
Zn(II)	biphasic system/ICP-OES[h]		1–160	0.4		4.8	
Cd(II)	D-μSPE/FAAS	Water, milk, and fruit juice	10–500	2.97	9.91	2.22	61
Zn(II)			5–500	1.55	5.17	1.97	
Cu(II)	D-μSPE[i]/HR-CS-AAS[j]	Food and water samples	10.4–1000	2.9	10.4	<5	62
Cd(II)	DSPME/FAAS	Hibiscus tea	10–150	3.8	12.8	—	63
Cd(II)	D-μSPE/FAAS	Water and food samples	—	25	83	1.9	64
Cd(II)	DLLME[k]/FAAS	Various water matrices and	0.08–370	0.024	0.08	1.8	65
Zn(II)		vegetable samples	2.5–560	0.76	2.5	2.2	
Cd(II)	D-μSPE/FAAS	Fruit juice samples	1.2–75	0.4	1.2	4.0	This work
Cu(II)			0.8–80	0.3	0.8	3.8	
Zn(II)			0.5–100	0.2	0.5	3.1	

[a] Linear range. [b] Limit of detection. [c] Limit of quantification. [d] Relative standard deviation. [e] Solid phase extraction/flame atomic absorption spectrometer. [f] Dispersive solid phase microextraction. [g] Dispersive micro solid phase extraction/energy dispersive X-ray fluorescence spectrometry. [h] Inductively coupled plasma-optical emission spectroscopy. [i] Dispersive solid phase extraction. [j] High resolution continuous source atomic absorption spectrometry. [k] Dispersive liquid–liquid microextraction.

interfere if it caused a change of ±5% in the ERs of the analytes. The results shown in Table 1 indicate that the ions likely present in real samples do not significant affect the extraction and determination of the analytes.

3.6. Method validation

The performance of the proposed method under optimal conditions was assessed by calculating quantitative parameters such as limit of detection (LOD), linear range (LR) of the calibration curve, limit of quantitation (LOQ), RSD, and ER. The linearity of the proposed method was evaluated through the construction of calibration curves after performing the developed procedure on ten standard solutions containing the analytes at various concentrations. The obtained calibration curves exhibited good linearity over the ranges of 0.8–80, 1.2–75, and 0.5–100 μg L^{-1} for Cu(II), Cd(II), and Zn(II) ions, respectively. LOD and LOQ were determined by dividing three times and ten times of standard deviation of blank measurements to the slope of the calibration curve, respectively. The LODs and LOQs were obtained in the ranges of 0.2–0.4 and 0.5–1.2 μg L^{-1}, respectively. The repeatability of the method expressed as RSD was obtained from repeated tests. To evaluate this parameter, two sets of experiments were conducted: (1) using the synthesized sorbent across six different solutions (C = 25 μg L^{-1} of each cation), and (2) employing the sorbent for extraction of the analytes for four different days. Intra-day precision (n = 6) resulted in RSDs of 4.0, 3.8, and 3.1%, while inter-day precision (n = 4) showed RSDs of 4.9, 4.8, and 3.7%, for Cd(II), Cu(II), and Zn(II) ions, respectively. The results are summarized in Table 2. To verify the accuracy of the developed method, concentrations of Cd(II), Cu(II), and Zn(II) ions were measured in a certified reference material (SPS-WW2 wastewater). The certified values alongside the results obtained are presented in Table 3, showing a good correlation between them.

3.7. Real samples analysis

To assess the repeatability and uniformity of the results, each juice sample was analyzed in triplicate, and the average values along with standard deviations were reported. The low RSD values (<5%) confirmed the satisfactory repeatability of the developed method for different fruit juice matrices. Prior to spiking, all fruit juice samples were analyzed to determine their native (pre-existing) levels of Cd(II), Cu(II), and Zn(II) ions. The detected concentrations were below the method detection limits or within the acceptable limits specified by food safety standards, indicating no significant background contamination among the samples. Although the juices were obtained from different domestic brands, no statistically significant differences were observed in the baseline metal contents (RSD < 5%), confirming comparable quality control across samples. The applicability of the proposed method was studied by determining Cd(II), Cu(II) and Zn(II) ions in seven fruit juice samples collected from different supermarkets. The results are collected in Table 4. Then to study matrix effects, the selected samples were spiked with Cd(II), Cu(II) and Zn(II) ions at two concentrations (10 and 50 μg L^{-1} of each) and were subjected to the developed extraction method. The recoveries obtained for the ions in the fruit juice were compared to the recoveries obtained in distilled water spiked with the similar concentrations and reported as relative recovery. The data are summarized in Table

Table 6 Key challenges and future research directions for nanocomposite-based extraction systems

Current challenges	Scientific description	Potential research innovations/future directions
Scale-up and reproducibility	Laboratory syntheses of MOF- and ZIF-based sorbents often suffer from poor reproducibility, complex multistep procedures, and high production costs, limiting industrial application	Development of continuous-flow, sol–gel, or green synthesis routes for scalable, reproducible, and cost-effective nanocomposite fabrication
Structural and chemical stability	ZIF/MOF frameworks can degrade in aqueous, acidic, or high-ionic-strength environments, reducing extraction performance in real matrices	Surface modification with silica, polymer, or carbon coatings to enhance hydrolytic stability and structural robustness
Regeneration and reusability	Active sites may become deactivated or blocked during repetitive adsorption–desorption cycles, leading to reduced extraction efficiency	Engineering self-cleaning, photoresponsive, or magnetically regenerable surfaces to prolong sorbent lifetime and maintain performance
Environmental sustainability	Accumulation or leaching synthetic nanomaterials raises potential ecological and toxicological concerns	Designing biodegradable, biochar-based, or eco-benign magnetic composites with low environmental impact
Selectivity in complex matrices	Coexisting ions and organic matters in food or environmental samples may compete for adsorption sites, affecting selectivity	Incorporation of selective ligands, molecularly imprinted layers, or functionalized frameworks for targeted metal-ions recognition

4. The average relative recoveries were in the range of 93.5–98.1% proved that the matrices of samples had no significant effect on the efficiency of the developed method.

3.8. Comparison of the method with other approaches

Several figures of merit consisting of LR, LOD, LOQ, and RSD for Cd(II), Cu(II) and Zn(II) ions obtained by the proposed method were compared with those of previous published methods and the results are listed in Table 5. According to the results, the method shows comparable/better LOQs and LODs compared to most of the other methods. The LR of the developed procedure is wider than the other methods. The RSD value of this study is comparable with the other methods.

4. Conclusions

In this study, a magnetic sorbent (SiO_2@ZIF-8@Fe_3O_4) was successfully synthesized and used as an efficient sorbent for the selective extraction and preconcentration of Cd(II), Cu(II) and Zn(II) ions from fruit juice samples. The sorbent combined the benefits of magnetic property of nanoparticles of Fe_3O_4 for easy separation, high surface area of ZIF-8 and high efficiency of SiO_2 for adsorption of heavy metal ions. This method achieved low LODs (0.2–0.4 μg L^{-1}) and LOQs (0.5–1.2 μg L^{-1}), wide LRs (0.5–100 μg L^{-1}) with good coefficients of determination (≥0.992), and high precision (RSD ≤ 4.0%). The developed method was successfully applied to different fruit juice samples and showed high recovery of the analytes and negligible matrix effects. Compared to other reported methods, this approach provided superior or comparable analytical performance for the determination of Cd(II), Cu(II) and Zn(II) ions in fruit juice samples. The high sensitivity and reliability of the method made it as a promising analytical tool for monitoring food safety and quality control in food industry. Future works can explore the extension of this approach to other heavy metals or food matrices, expanding its potential applications in food analysis. Although the synthesized SiO_2@ZIF-8@Fe_3O_4 nanocomposite exhibited remarkable analytical performance, several critical challenges still need to be addressed to facilitate its broader practical implementation. These challenges include the scalable and cost-effective synthesis of the nanocomposite, ensuring long-term structural and chemical stability in complex matrices, improving sorbent regeneration and reusability, and mitigating potential environmental concerns associated with nanomaterial residues. Future research should therefore focus on developing greener and more sustainable synthesis strategies, enhancing sorbent recyclability and durability, designing multifunctional hybrid materials (*e.g.*, carbon-based or ion-exchange composites), and integrating the extraction procedure with advanced detection systems such as ICP-MS or electrochemical sensors to further enhance sensitivity and analytical throughput. Table 6 summarizes the major challenges associated with nanocomposite-based extraction systems and highlights potential research directions for overcoming them.

Conflicts of interest

The authors declare that there are no conflicts of interest.

Data availability

All data generated or analyzed during this study are included in this published article. This data is provided within the manuscript file.

Acknowledgements

Saeed Mohammad Sorouraddin has received research grants from University of Tabriz. The authors thank the Research Council of the University of Tabriz for financial support.

References

1 A. Hazrat, E. Khan and I. Ilahi, *J. Chem.*, 2019, **2019**, 6730305.
2 N. D. Takarina, A. I. S. Purwiyanto and Y. Suteja, *Mar. Pollut. Bull.*, 2021, **170**, 112607.
3 S. Mitra, A. J. Chakraborty, A. M. Tareq, T. B. Emran, F. Nainu, A. Khusro, M. I. Abubakr, M. U. Khandaker, H. Osman and F. A. Alhumaydhi, *J. King Saud Univ. Sci.*, 2022, **34**, 101865.
4 N. Munir, M. Jahangeer, A. Bouyahya, N. El Omari, R. Ghchime, A. Balahbib, S. Aboulaghras, Z. Mahmood, M. Akram, S. M. Ali Shah, I. N. Mikolaychik, M. Derkho, M. Rebezov, B. Venkidasamy, M. Thiruvengadam and M. A. Shariati, *Sustainability*, 2021, **14**, 161.
5 Y. Lei, M. Guo, J. Xie, X. Liu, X. Li, H. Wang, Y. Xu and D. Zheng, *Front. Endocrinol.*, 2024, **15**, 1354577.
6 H. Schoofs, J. Schmit and L. Rink, *Molecules*, 2024, **29**, 3130.
7 D. Tibebe, M. Hussen, M. Mulugeta, D. Yenealem, Z. Moges, M. Gedefaw and Y. Kassa, *BMC Chem. Biol.*, 2022, **16**, 87.
8 M. Hejazi, P. Jamshidi and F. Shemirani, *Res. Chem. Intermed.*, 2021, **47**, 3867–3881.
9 I. Y. Ikhsani, B. Kumayanjati, E. N. Dida and S. Y. Cahyarini, *J. Phys. Conference Series*, 2022, **2377**, 012039.
10 S. V. Smirnova, D. V. Ilin and I. V. Pletnev, *Talanta*, 2021, **221**, 121485.
11 P. Ali Mohammadzadeh Baghaei, M. R. Afshar Mogaddam, M. A. Farajzadeh, A. Mohebbi and S. M. Sorouraddin, *J. Food Compos. Anal.*, 2023, **117**, 105125.
12 S. Y. Kwon, Y. I. Kim, Y. K. Kim, Y. B. Lee and J. H. Mok, *LWT*, 2024, **208**, 116708.
13 S. O. O. John, S. F. Olukotun, T. G. Kupi and M. Mathuthu, *Appl. Water Sci.*, 2024, **14**, 202.
14 A. Najla, M. A. Habila, Z. A. Alothman, T. S. Alomar, N. Alraqibah, M. Sheikh, A. A. Ghfar and M. Soylak, *Anal. Methods*, 2020, **12**, 4949.
15 E. Leburu, Y. Qiao, Y. Wang, Y. Jiakuan, Sh. Liang, W. Yu, Sh. Yuan, H. Duan, L. Huang, J. Hu and H. Hou, *Biomed. Microdevices*, 2024, **26**, 30.
16 R. R. Pasupuleti and Y. L. Huang, *J. Chin. Chem. Soc.*, 2023, **70**, 1326.
17 M. Jin, H. Yuan, B. Liu, J. Peng, L. Xu and D. Yang, *Anal. Methods*, 2020, **12**, 5747.
18 L. E. Hosry, N. Sok, R. Richa, L. A. Mashtoub, P. Cayot and E. Bou-Maroun, *Foods*, 2023, **12**, 895.
19 S. P. Padinhattath and R. L. Gardas, *Separ. Purif. Technol.*, 2025, **356**, 129880.
20 G. S. Nyamato, K. Wambugua, J. Kiratua and S. O. Ojwach, *Water Sci. Technol.*, 2022, **85**, 2993.
21 P. Liang, R. Liu and J. Cao, *Microchim. Acta*, 2008, **160**, 135–139.
22 W. Ali Khan, M. B. Arain, Y. Yamini, N. Shah, T. Gul Kazi, S. Pedersen-Bjergaard and M. Tajik, *J. Pharm. Anal.*, 2020, **10**, 109–122.
23 N. Mafakheri, M. Shamsipur and N. Babajani, *Microchem. J.*, 2024, **199**, 110010.
24 M. A. Farajzadeh, L. Khoshmaram and M. R. Afshar Mogaddam, *J. Sep. Sci.*, 2015, 2470–2487.
25 T. Shahryari, P. Singh, P. Raizada, A. Davidyants, L. Thangavelu, S. Sivamani, A. Naseri, F. Vahidipour, A. Ivanets and A. Hosseini Bandegharaei, *Colloids Surf., A*, 2022, **641**, 128528.
26 N. Kobylinska, L. Kostenko, S. Khainakov and S. Garcia-Granda, *Microchim. Acta*, 2020, **187**, 289.
27 X. Dong, X. Gao, J. Song and L. Zhao, *Food Chem.*, 2021, **360**, 130023.
28 S. Jabbari, S. M. Sorouraddin, M. A. Farajzadeh and Afshar Mogaddam, *Sci. Rep.*, 2025, **15**, 32235.
29 A. Bakhshi, S. M. Sorouraddin, Afshar Mogaddam and M. A. Farajzadeh, *J. Food Compos. Anal.*, 2025, **144**, 107649.
30 Q. Zhou, T. Yu, R. Yang, X. Guo and Y. Chen, *ACS Omega*, 2025, **10**, 47790–47801.
31 Y. Huang, X. Zeng, L. Guo, J. Lan, L. Zhang and D. Cao, *Sep. Purif. Technol.*, 2018, **194**, 462–469.
32 Y. Zhang, Zh. Xie, Zh. Wang, X. Feng, Y. Wang and A. Wu, *Dalton Trans.*, 2016, **45**, 12653–12660.
33 T. T. Bui, D. C. Nguyen, S. H. Hua, H. Chun and Y. S. Kim, *Nanomaterials*, 2022, **12**, 753.
34 X. Jiang, S. Su, J. Rao, S. Li, T. Lei, H. Bai and X. Yang, *J. Environ. Chem. Eng.*, 2021, **9**, 105959.
35 X. Meng, Z. Lv, L. Shi, T. Jiang, S. Sun, Y. Li and J. Feng, *ACS Appl. Nano Mater.*, 2023, **6**, 6581–6593.
36 N. Sheraz, A. Shah, A. Haleem and F. J. Iftikhar, *RSC Adv.*, 2024, **14**, 11284.
37 I. Pet, M. N. Sanad, M. Farouz, M. M. ElFaham, A. El-Hussein, M. S. Abd El-sadek, R. A. Althobiti and A. Ioanid, *Water Conserv. Sci. Eng.*, 2024, **9**, 62.
38 S. Pourbeyram, *Ind. Eng. Chem. Res.*, 2016, **55**, 5608–5617.
39 W. Peng, H. Li, Y. Liu and S. Song, *J. Mol. Liq.*, 2017, **230**, 496–504.
40 J. Bayar, N. Ali, Y. Dong, U. Ahmad, M. M. Anjum, G. R. Khan, M. Zaib, A. Jalal, R. Ali and L. Ali, *Environ. Geochem. Health*, 2024, **46**, 428.
41 B. Qiu, X. Tao, H. Wang, W. Li, X. Ding and H. Chu, *J. Anal. Appl. Pyrolysis*, 2021, **155**, 105081.
42 R. Mirzajani and M. Dianati, *Desalination Water Treat.*, 2025, **321**, 101060.
43 S. V. Pochampally, J. Gonzalez Blanco, K. Ayalew, S. E. H. Murph and J. Moon, *Sep. Purif. Technol.*, 2024, **350**, 127793.
44 Q. Wu, D. Wang, C. Chen, C. Peng, D. Cai and Z. Wu, *J. Environ. Manage.*, 2021, **290**, 112626.
45 X. Liu, R. Ma, X. Wang, Y. Ma, Y. Yang, L. Zhuang, S. Zhang, R. Jehan, J. Chen and X. Wang, *Environ. Pol.*, 2019, **252**, 62–73.
46 M. Babazadeh, R. Hosseinzadeh-Khanmiri, J. Abolhasani, E. Ghorbani-Kalhora and A. Hassanpour, *RSC Adv.*, 2015, **5**, 19884–19892.
47 M. Soylak and Y. E. Unsal, *Environ. Monit. Assess.*, 2011, **181**, 577–586.
48 R. Jayalakshmi, J. Jeyanthi and K. R. Aswin Sidhaarth, *Environ. Nanotechnol. Monit. Manag.*, 2022, **17**, 100659.

49 T. T. Nguyen, T. H. D. Nguyen, T. T. T. Huynh, M. H. D. Dang, L. H. T. Nguyen, T. L. H. Doan, T. P. Nguyen, M. A. Nguyen and P. H. Tran, *RSC Adv.*, 2022, **12**, 19741–19750.
50 S. G. Ali, S. Kapoor, R. A. Khan, U. Haseen and H. M. Khan, *RSC Adv.*, 2024, **14**, 34556–34564.
51 P. Rana, B. Kaur, K. Poonia, V. Soni, P. Singh, S. Thakur, C. W. Huang, V. H. Nguyen and P. Raizada, *Inorg. Chem. Commun.*, 2025, **172**, 113657.
52 P. Montoro-Leal, J. C. García-Mesa, M. T. Siles Cordero, M. M. López Guerrero and E. Vereda Alonso, *Microchem. J.*, 2020, **155**, 104796.
53 I. Hagarová and L. Nemček, *Crit. Rev. Anal. Chem.*, 2024, **54**, 3114.
54 M. Öner, S. Bodur, C. Demir, E. Yazıcı, S. Erarpat and S. Bakırdere, *J. Food Compos. Anal.*, 2021, **101**, 103978.
55 X. Wei, A. Gopal, T. Chen, S. Chen, L. Ding, Q. Jia, A. Lewis, F. S. Butt, Z. Chen, R. Krishnamoorthi, N. Radacsi, C. H. Lau, X. Chen, S. Yang and Y. Huang, *Separ. Purif. Technol.*, 2025, **357**, 130031.
56 H. Liu, S. Ji, Y. Zheng, M. Li and H. Yang, *Powder Technol.*, 2013, **246**, 520.
57 A. Islam, S. Kumar, N. Zaidi and H. Ahmad, *Food Chem.*, 2016, **213**, 775.
58 I. H. Alsohaimi, M. A. Kariri, M. Alzaid, M. S. Alhumaimess, M. Y. El- Sayed, M. S. Alshammari, E. K. Alenezy and H. M. A. Hassan, *J. Mol. Liq.*, 2024, **393**, 123663.
59 K. Pytlakowska, M. Matussek, B. Hachuła, M. Pilch, K. Kornaus, M. Zubko and W. A. Pisarski, *Spectrochim. Acta, Part B*, 2018, **147**, 79.
60 S. V. Smirnova, D. V. Ilin and I. V. Pletnev, *Talanta*, 2021, **221**, 121485.
61 T. Mumcu, S. Oncuoglu, C. G. Hızlıates and S. S. Bozkurt, *J. Food Compos. Anal.*, 2025, **143**, 107638.
62 M. Soylak, A. M. A. Mohammed and F. Uzcan, *J. Food Compos. Anal.*, 2025, **144**, 107733.
63 C. Demir, M. Oner, G. Çetin and T. Bakırdere, *J. Food Compos. Anal.*, 2024, **127**, 105968.
64 M. Soylak, M. Issufo and O. Ozalp, *J. Food Compos. Anal.*, 2025, **148**, 108173.
65 A. T. Bisgin, A. Elik and N. Altunay, *Microchem. J.*, 2025, **216**, 114790.